J Eng Math (2007) 59:301–321
DOI 10.1007/s10665-006-9113-7

ORIGINAL PAPER

Constrained optimization for interface cracks in composite materials subject to non-penetration conditions

M. Hintermüller · V. A. Kovtunenko · K. Kunisch

Received: 20 March 2006 / Accepted: 13 September 2006 / Published online: 24 November 2006

Abstract A constrained problem for a composite material with an interface crack subject to non-penetration conditions is considered. The response of a composite consisting of two identical homogeneous orthotropic materials is described with respect to in-plane deformation. The coupling of the materials occurs at an interface with angle between their vertical planes of elastic symmetry. The model is not split into independent in-plane and anti-plane states. Well-posedness of the problem is proved by variational methods. For numerical computations, a semi-smooth Newton method is proposed and its convergence is studied. Using the proposed algorithms, numerical experiments for an interface crack under mode-3 loading are presented and analyzed with respect to the half-angle defining the coupling.

Keywords Composite material · Constrained optimization · Interface crack · Semi-smooth Newton methods · Variational methods

1 Introduction

Problems with cracks in fracture mechanics are important for the design of structures in engineering sciences. A mathematical formulation of these problems can be developed within the framework of elasticity [1–3]. Because of the presence of a crack in the domain, singular solutions are possible. In the three-dimensional case, the nature of singularities is still subject to research. To gain insight into the three-dimensional situation, the standard approach is to simplify the elasticity model by splitting it into two two-dimensional, in-plane and anti-plane, models. However, this leads to a loss of information concerning the three-dimensional nature of the system. Some experimental investigations in this direction can be found in [4]. To address these drawbacks, we introduce an intermediate 2.5-dimensional model instead of

M. Hintermüller (✉) · V. A. Kovtunenko · K. Kunisch
Department of Mathematics, University of Graz, 8010 Graz, Austria
e-mail: michael.hintermueller@uni-graz.at

K. Kunisch
e-mail: karl.kunisch@uni-graz.at

V. A. Kovtunenko
Lavrent'ev Institute of Hydrodynamics, 630090 Novosibirsk, Russia
e-mail: kovtunenko@hydro.nsc.ru

the splitting approach. Although our model takes into account all three components of the displacement vector, it is formulated in a two-dimensional domain. This model is well suited also for the analysis of the delamination of a composite with an interface crack. For the formulation of elasticity models in composite laminates see [5].

For the construction of the 2.5-dimensional model, we consider a homogeneous orthotropic material with a vertical plane of elastic symmetry rotated by an angle of β with respect to a reference coordinate system. As a specific case, we consider a semi-isotropic material that is fibered along a fixed direction having angle β with the x_3-axis and is isotropic in all orthogonal cross-sections. We compose two pieces of such a material along the interface $x_2 = 0$ such that the corresponding angles in the upper and lower half-spaces are β and $-\beta$, respectively. We further assume that a crack is situated along a part of the interface. Applying the assumption of plain deformation at $x_3 = \text{const}$, due to the rotation, we obtain a spatial model.

In our numerical experiments we observe three-dimensional effects: mixing of crack modes (mode-1 with mode-3), and contact between opposite crack surfaces. They occur under pure mode-3 loading, which is ruled out for the in-plane and anti-plane models. Due to the latter phenomenon, we are required to consider (unilaterally) constrained crack problems with non-penetration conditions. The inequality constraint imposed on the jump of the displacement at opposite crack faces prevents the non-physical and thus inconsistent behavior of overlapping faces that may occur in the linear setting of the crack problem. The mathematical formulation results in a variational inequality. An account for the variational techniques for crack problems can be found in [6,7]. The variational formulation provides the appropriate state space with a singularity at the crack tip.

For plane models, the general approach for the analysis of singularities between two anisotropic half-planes was described in [8]. The elastic problem determining the corresponding singular solutions can be reduced with the help of a partial Fourier transformation and the Stroh formalism to a matrix eigenvalue problem. An analytic realization of such a complicated technique is available only for particular cases. The analytical solutions obtained in [8] require suitable orientation of the axes of material symmetry to ensure decoupling of the anti-plane fracture mode from the in-plane modes. Alternatively, in [9] an eigenvalue problem for power solutions (singular solutions of a specific form) was treated as a self-adjoint system to formally derive the order of the singularity and to define its eigenvectors with no assumption of symmetry.

We shall investigate the geometric and physical features of the composite model by numerical experiments. For this purpose, a semi-smooth Newton technique is adapted to constrained crack problems. As a general rule, variational problems subject to unilateral constraints (the non-penetration conditions in our case) are not Fréchet-differentiable with respect to the dual variable. This requires non-smooth optimization techniques [10–12]. Under suitable assumptions, semi-smoothness concepts will allow a locally superlinear convergence of the Newton iterates. Such properties are not available for problems with cracks due to the lack of regularity caused by the geometric singularities of a domain with a crack.

If we restrict our attention to the discretized problem, we arrive at a finite-dimensional linear complementarity problem (see [13]). In this case, superlinear convergence of the semi-smooth Newton method can be proved. Moreover, in numerical experiments, global and monotone convergence was observed, which is supported by the *a posteriori* analysis in [14]. For a class of variational problems subject to boundary constraints, an argument was developed in [15] based on perturbation of M-matrices guaranteeing these convergence properties.

Returning to the continuous setting of the problem, a penalization technique was utilized in [16] to obtain an approximate Lagrange multiplier, which enjoys extra L^p-regularity. As a consequence, the generalized differentiability and the local superlinear convergence rate of the Newton iterates were derived for the penalized problem in function space.

For the problems under consideration, semi-smooth Newton methods are equivalent to primal–dual active-set algorithms [17,18]. They are an efficient tool for the numerical treatment of constrained variational problems. As suggested by the terminology, these algorithms use the primal as well as the

dual variables independently to find the active (contact part of the crack surfaces) and the inactive (non-contact part) sets of the solution. In numerical examples, the primal–dual active-set methods turned out to produce the exact numerical solution in only a few (typically $\leq$12) iterations, even in degenerate cases where pure primal methods may chatter. In comparison to interior-point methods, see, e.g., [19], the primal–dual active-set strategy determines not an approximate, but the exact solution of the discrete problem. Decreasing the mesh-size results only in a moderate increase of the required number of iterations. We will suggest a combination of a local grid-refinement near the crack with a continuation technique reducing costly fine-grid iterations. For further numerical aspects we refer to, e.g., [20], where a convergence analysis of a finite-element discretization of a related crack problem is provided, and to [21,22], where extended finite-element techniques are used for curvilinear cracks.

2 Constrained crack problems for a composite

In this section, we formulate a model with respect to an in-plane deformation of two identical homogeneous orthotropic materials with a planar interface and a crack along part of their interface. The specific cases of material parameters for fibered, isotropic, and orthotropic solids are described in the Appendix. Based on the corresponding representation of elasticity coefficients on constitutive and equilibrium laws, we deduce the variational setting of the problem.

2.1 Modeling of composite materials in plane deformation

Consider a homogeneous orthotropic material with planes of elastic symmetry corresponding to the (x_1', x_2', x_3')-axes, which can be described by nine independent (positive) material parameters (see [23]):

$$E_1,\ E_2,\ E_3,\ \nu_{21},\ \nu_{32},\ \nu_{31},\ G_{21},\ G_{32},\ G_{31}. \tag{2.1}$$

First, we compose the identical materials with respect to a reference coordinate system (x_1, x_2, x_3) in the following way. In the "upper" half-space, $\mathbb{R}^3_+ = \{x_1, x_2 \geq 0, x_3\}$, the (x_1', x_2', x_3')-axes are rotated in the clockwise direction to (x_1, x_2, x_3) with respect to the common $x_2' = x_2$-axis by the angle β between x_3' and x_3. The angle $\beta \in [-\pi/2, \pi/2]$ is arbitrarily fixed. In the "lower" half-space, $\mathbb{R}^3_- = \{x_1, x_2 \leq 0, x_3\}$, the (x_1', x_2', x_3')-axes are rotated to (x_1, x_2, x_3) with respect to $x_2' = x_2$ in the opposite direction by the same angle (i.e., $-\beta$), as illustrated in Fig. 1. The materials are assumed to be joined along the plane $x_2 = 0$ with an interface defect (crack).

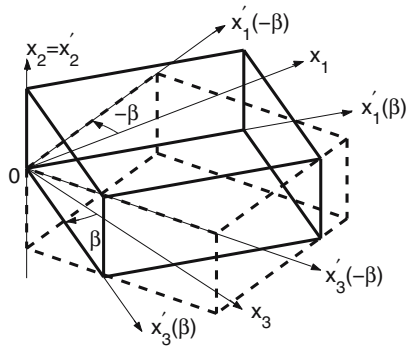

Fig. 1 Composition of a body in $\mathbb{R}^3_\pm$

For a displacement vector $u = (u_1, u_2, u_3)^\top(x)$ (at a point $x = (x_1, x_2, x_3)^\top \in \mathbb{R}^3$) in the composite material,

$$u = \begin{cases} u^+ & \text{in } \mathbb{R}^3_+, \\ u^- & \text{in } \mathbb{R}^3_-, \end{cases}$$

we introduce a strain tensor $\varepsilon = \{\varepsilon_{ij}\}$ according to the linear Cauchy law,

$$\varepsilon_{ij}(u) = 0.5(u_{i,j} + u_{j,i}), \quad i,j = 1,2,3, \tag{2.2}$$

and a 3×3 symmetric tensor of stress $\sigma = \{\sigma_{ij}\}$,

$$\sigma(u) = \begin{cases} \sigma^\beta(u^+) & \text{in } \mathbb{R}^3_+, \\ \sigma^{-\beta}(u^-) & \text{in } \mathbb{R}^3_-. \end{cases} \tag{2.3}$$

Here and throughout we utilize the standard tensor notation common in linear elasticity and the summation convention for the repeated indices $i,j = 1,2,3$.

Second, we apply the assumption of plane deformation at every cross-section $x_3 = \text{const}$, which means that none of the three components of the displacement vector u depends on x_3. Hence $\varepsilon_{33} = 0$, and the strain tensor in (2.2) takes the particular form

$$\begin{aligned} &\varepsilon_{11}(u) = u_{1,1}, \quad \varepsilon_{22}(u) = u_{2,2}, \\ &\varepsilon_{12}(u) = 0.5(u_{1,2} + u_{2,1}), \\ &\varepsilon_{13}(u) = 0.5u_{3,1}, \quad \varepsilon_{23}(u) = 0.5u_{3,2}. \end{aligned} \tag{2.4}$$

In $\mathbb{R}^3_+$, the relevant components of the stress tensor (2.3) satisfy the following constitutive relations involving a non-symmetric matrix:

$$\begin{bmatrix} \sigma^\beta_{11} \\ \sigma^\beta_{22} \\ \sigma^\beta_{12} \\ \sigma^\beta_{23} \\ \sigma^\beta_{13} \end{bmatrix} = \begin{bmatrix} C^\beta_{11} & C^\beta_{12} & 0 & 0 & 2C^\beta_{16} \\ C^\beta_{12} & C_{22} & 0 & 0 & 2C^\beta_{26} \\ 0 & 0 & 2C^\beta_{44} & 2C^\beta_{45} & 0 \\ 0 & 0 & 2C^\beta_{45} & 2C^\beta_{55} & 0 \\ C^\beta_{16} & C^\beta_{26} & 0 & 0 & 2C^\beta_{66} \end{bmatrix} \begin{bmatrix} \varepsilon_{11} \\ \varepsilon_{22} \\ \varepsilon_{12} \\ \varepsilon_{23} \\ \varepsilon_{13} \end{bmatrix} \tag{2.5}$$

with nine elasticity coefficients depending on β (except for C_{22}) and the material parameters (2.1) as presented in the Appendix. Substituting (2.4) in (2.5) allows us to rewrite the constitutive law in the symmetric form:

$$\begin{aligned} \sigma^\beta_{11}(u) &= C^\beta_{11}u_{1,1} + C^\beta_{12}u_{2,2} + C^\beta_{16}u_{3,1}, \\ \sigma^\beta_{22}(u) &= C^\beta_{12}u_{1,1} + C_{22}u_{2,2} + C^\beta_{26}u_{3,1}, \\ \sigma^\beta_{12}(u) &= C^\beta_{44}(u_{1,2} + u_{2,1}) + C^\beta_{45}u_{3,2}, \\ \sigma^\beta_{23}(u) &= C^\beta_{45}(u_{1,2} + u_{2,1}) + C^\beta_{55}u_{3,2}, \\ \sigma^\beta_{13}(u) &= C^\beta_{16}u_{1,1} + C^\beta_{26}u_{2,2} + C^\beta_{66}u_{3,1}. \end{aligned} \tag{2.6}$$

In $\mathbb{R}^3_-$ the above relations hold true if we exchange β with $-\beta$ according to (2.3). The elasticity coefficients obey the following symmetry properties (see the Appendix):

$$\begin{aligned} &C^{-\beta}_{11} = C^\beta_{11}, \quad C^{-\beta}_{12} = C^\beta_{12}, \quad C^{-\beta}_{44} = C^\beta_{44}, \quad C^{-\beta}_{55} = C^\beta_{55}, \quad C^{-\beta}_{66} = C^\beta_{66}, \\ &C^{-\beta}_{16} = -C^\beta_{16}, \quad C^{-\beta}_{26} = -C^\beta_{26}, \quad C^{-\beta}_{45} = -C^\beta_{45}. \end{aligned} \tag{2.7}$$

Note that if $\beta = 0$ or $\beta = \pm\pi/2$, then we have $C^\beta_{16} = C^\beta_{26} = C^\beta_{45} = 0$, and (2.6) is split into two independent states, namely the in-plane state for $(u_1, u_2)^\top$ and the anti-plane state for u_3. If $\beta \neq 0, \pm\pi/2$ then we have a spatial model.

2.2 Equilibrium problem for the interface crack with non-penetration conditions

Consider the composite of two elastic orthotropic materials joined along the plane $x_2 = 0$, described in Sect. 2.1. Assume that in each cross-section $x_3 = \text{const}$, the solid occupies a domain $\Omega \subset \mathbb{R}^2$ consisting of two sub-domains $\Omega^+ \subset \mathbb{R}^2_+$ and $\Omega^- \subset \mathbb{R}^2_-$, with the interface Σ located on the line $x_2 = 0$, i.e., $\Omega = \Omega^+ \cup \Omega^- \cup \Sigma$. Let Ω be bounded by the Lipschitz boundary $\partial\Omega = \Gamma_N \cup \Gamma_D$ with an outward normal vector $n = (n_1, n_2)^\top$, where $\Gamma_D \neq \emptyset$. We suppose that the crack Γ_C is part of the interface Σ, and define the domain with the crack as $\Omega_C = \Omega \setminus \overline{\Gamma}_C$. Its boundary $\partial\Omega_C$ is the union of Γ_N, Γ_D, and the crack surfaces $\Gamma_C^\pm$. Here $\Gamma_C^+ \subset \Sigma^+$ and $\Gamma_C^- \subset \Sigma^-$ are defined as the limit points of sequences $\{x_n\} \in \Omega^+$ and $\{x_n\} \in \Omega^-$ at Σ, respectively.

To prevent mutual inter-penetrations between the opposite crack surfaces Γ_C^+ and Γ_C^-, we impose a non-negativity condition on the jump of the displacement normal to the crack (u_2-component); see [6]. Let $g = (g_1, g_2, g_3)^\top$ represent a surface traction given at Γ_N; without loss of generality, assume that the volume force is zero. Further, the solid is assumed to be fixed at Γ_D. The problem of equilibrium of the composite with a crack is finally described by the following nonlinear (at Γ_C) relations:

$$
\begin{aligned}
&-\sigma_{1\alpha,\alpha}(u) = -\sigma_{2\alpha,\alpha}(u) = -\sigma_{3\alpha,\alpha}(u) = 0 \quad \text{in } \Omega_C,\\
&\sigma_{12}(u) = \sigma_{23}(u) = 0 \quad \text{on } \Gamma_C^\pm,\\
&[\![\sigma_{22}(u)]\!] = 0,\ [\![u_2]\!] \geq 0,\ \sigma_{22}(u) \leq 0,\ \sigma_{22}(u)[\![u_2]\!] = 0 \quad \text{on } \Gamma_C,\\
&[\![u_1]\!] = [\![u_2]\!] = [\![u_3]\!] = 0,\\
&[\![\sigma_{12}(u)]\!] = [\![\sigma_{22}(u)]\!] = [\![\sigma_{23}(u)]\!] = 0 \qquad \text{on } \Sigma \setminus \Gamma_C,\\
&\sigma_{1\alpha}(u)n_\alpha = g_1,\ \sigma_{2\alpha}(u)n_\alpha = g_2,\ \sigma_{3\alpha}(u)n_\alpha = g_3 \quad \text{on } \Gamma_N,\\
&u_1 = u_2 = u_3 = 0 \quad \text{on } \Gamma_D,
\end{aligned}
\tag{2.8}
$$

where the summation convention over repeated indices $\alpha = 1, 2$ is used. Here $[\![u]\!] = u^+ - u^-$ and $[\![\sigma(u)]\!] = \sigma^\beta(u^+) - \sigma^{-\beta}(u^-)$ denote the jumps across the interface.

In view of (2.6) and (2.7), the divergence of the stress used in (2.8) has the following representation in $\Omega^\pm$:

$$
\begin{aligned}
\sigma^{\pm\beta}_{1\alpha,\alpha}(u^\pm) &= C^\beta_{11}u^\pm_{1,11} + C^\beta_{44}u^\pm_{1,22} + (C^\beta_{12} + C^\beta_{44})u^\pm_{2,12} \pm C^\beta_{16}u^\pm_{3,11} \pm C^\beta_{45}u^\pm_{3,22},\\
\sigma^{\pm\beta}_{2\alpha,\alpha}(u^\pm) &= (C^\beta_{12} + C^\beta_{44})u^\pm_{1,12} + C^\beta_{44}u^\pm_{2,11} + C_{22}u^\pm_{2,22} \pm (C^\beta_{45} + C^\beta_{26})u^\pm_{3,12},\\
\sigma^{\pm\beta}_{3\alpha,\alpha}(u^\pm) &= \pm C^\beta_{16}u^\pm_{1,11} \pm C^\beta_{45}u^\pm_{1,22} \pm (C^\beta_{45} + C^\beta_{26})u^\pm_{2,12} + C^\beta_{66}u^\pm_{3,11} + C^\beta_{55}u^\pm_{3,22}.
\end{aligned}
\tag{2.9}
$$

2.3 Constrained variational problem with a crack

Next we study the nonlinear boundary-value problem (2.8) within a variational framework. Due to the non-penetration conditions, this results in a variational inequality; see (2.13).

For this purpose, let us introduce the cone of admissible displacements which accounts for all boundary conditions imposed on u in (2.8) as

$$
\begin{aligned}
&K(\Omega_C) = \{u \in H(\Omega_C) :\ [\![u_2]\!] \geq 0 \quad \text{on } \Gamma_C\} \quad \text{with}\\
&H(\Omega_C) = \{u \in H^1(\Omega_C)^3 :\ u = 0 \quad \text{on } \Gamma_D\}.
\end{aligned}
$$

For given $g \in L^2(\Gamma_N)^3$, the potential energy of the composite with a crack is defined by

$$
\Pi(u) = \frac{1}{2}\int_{\Omega_C} \sigma_{ij}(u)\varepsilon_{ij}(u)\,\mathrm{d}x - \int_{\Gamma_N} g_i u_i\,\mathrm{d}s, \tag{2.10}
$$

where, due to (2.4), (2.6), and (2.7), the quadratic form has the representation in $\Omega^{\pm}$ (recall that $\varepsilon_{33} = 0$):

$$\begin{aligned}\sigma_{ij}^{\pm\beta}(u^{\pm})\varepsilon_{ij}(u^{\pm}) = {} & C_{11}^{\beta}(u_{1,1}^{\pm})^2 + C_{22}(u_{2,2}^{\pm})^2 + 2C_{12}^{\beta}u_{1,1}^{\pm}u_{2,2}^{\pm} \pm 2C_{16}^{\beta}u_{1,1}^{\pm}u_{3,1}^{\pm} \\ & \pm 2C_{26}^{\beta}u_{2,2}^{\pm}u_{3,1}^{\pm} + C_{44}^{\beta}(u_{1,2}^{\pm} + u_{2,1}^{\pm})^2 \pm 2C_{45}^{\beta}(u_{1,2}^{\pm} + u_{2,1}^{\pm})u_{3,2}^{\pm} \\ & + C_{55}^{\beta}(u_{3,2}^{\pm})^2 + C_{66}^{\beta}(u_{3,1}^{\pm})^2. \end{aligned} \tag{2.11}$$

The weak solution $u \in K(\Omega_C)$ to the equilibrium problem (2.8) is defined as the solution of the constrained minimization problem

$$\text{minimize } \Pi(v) \quad \text{over } v \in K(\Omega_C). \tag{2.12}$$

The optimality condition to (2.12) is expressed by the variational inequality

$$\int_{\Omega_C} \sigma_{ij}(u)\varepsilon_{ij}(v-u)\,\mathrm{d}x \geq \int_{\Gamma_N} g_i(v-u)_i\,\mathrm{d}s \quad \text{for all } v \in K(\Omega_C). \tag{2.13}$$

For unique solvability of (2.12) (or equivalently (2.13)) uniform positivity of the quadratic term is needed, i.e., the existence of an angle β and a constant $c_0(\beta) > 0$ such that

$$\int_{\Omega_C} \sigma_{ij}(u)\varepsilon_{ij}(u)\,\mathrm{d}x \geq c_0(\beta)\|u\|^2_{H(\Omega_C)} \quad \text{for every } u \in H(\Omega_C) \tag{2.14}$$

holds. If the 5×5-matrix in (2.6) is positive definite for all β, as will be the case in the example given below, then this leads to the estimate:

$$\int_{\Omega_C} \sigma_{ij}(u)\varepsilon_{ij}(u)\,\mathrm{d}x \geq \lambda_{\min}(\beta) \int_{\Omega_C} \varepsilon_{ij}(u)\varepsilon_{ij}(u)\,\mathrm{d}x \tag{2.15}$$

with the minimal eigenvalue $\lambda_{\min}(\beta) > 0$ of this matrix. In this case, a Korn-type argument based on (2.15) implies (2.14).

It can be verified for the solution u of (2.13) that $[\![u]\!] \in H_{00}^{1/2}(\Gamma_C)^3$, where $H_{00}^{1/2}(\Gamma_C)$ is the space of functions in $H^{1/2}(\Gamma_C)$ that admit a continuation by zero on an extension of Γ_C into Ω_C. Since the trace of $H(\Omega_C)$ onto $H_{00}^{1/2}(\Gamma_C)^3$ is surjective, we can define a unique Lagrange multiplier $\lambda \in H_{00}^{1/2}(\Gamma_C)^\star$ such that

$$\int_{\Omega_C} \sigma_{ij}(u)\varepsilon_{ij}(v)\,\mathrm{d}x - \langle \lambda, [\![v_2]\!]\rangle_{\Gamma_C} = \int_{\Gamma_N} g_i v_i\,\mathrm{d}s \quad \text{for all } v \in H(\Omega_C), \tag{2.16a}$$

$$\langle \lambda, \xi - [\![u_2]\!]\rangle_{\Gamma_C} \geq 0 \quad \text{for all } 0 \leq \xi \in H_{00}^{1/2}(\Gamma_C), \tag{2.16b}$$

where $\langle\cdot,\cdot\rangle_{\Gamma_C}$ stands for the duality pairing between the spaces $H_{00}^{1/2}(\Gamma_C)$ and $H_{00}^{1/2}(\Gamma_C)^\star$. Conversely, for every solution $(u,\lambda)^\top \in H(\Omega_C) \times H_{00}^{1/2}(\Gamma_C)^\star$ of (2.16), the first component u satisfies (2.13). Moreover, applying Green's formula to the first term in (2.13) and using (2.16a), we arrive at the identity

$$\sigma_{22}^{\beta}(u^+) = \sigma_{22}^{-\beta}(u^-) = -\lambda \quad \text{on } \Gamma_C^{\pm}. \tag{2.17}$$

Thus (2.16) yields the primal–dual variational formulation of the equilibrium problem (2.8).

2.4 Observations for a nonlinear model

Before developing a discretization of the problem and describing a numerical algorithm for the solution, we give an illustrative example that clarifies principal features of the system under consideration.

We choose the following symmetric geometry for the composite with a crack of length $l = 0.75$ loaded by the pair of anti-symmetric traction forces g_0, as presented in Fig. 2. Its detailed description is given in Sect. 3.3. The fibering directions are marked in Fig. 2 with parallel solid lines. For calculations, the angle β of fibering is taken at the six points $\beta = 0, \pi/16, \pi/8, \pi/4, 3\pi/8, \pi/2$ in $[0, \pi/2]$. This includes the limit

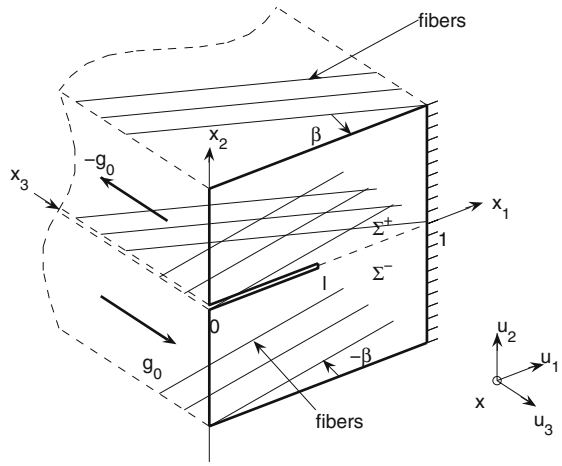

Fig. 2 An example configuration

cases of the plane isotropic model with $\beta = 0$, and the plane orthotropic model with $\beta = \pi/2$. Note that for $\beta = \pi/4$, the directions of fibering in Ω^+ and Ω^- are mutually orthogonal.

For $l = 0.75$, the components of displacements u_1, u_2, u_3 and the stresses $\sigma_{12}(u), \sigma_{22}(u), \sigma_{23}(u)$ at the interface surfaces $\Sigma^{\pm}$ are depicted in Fig. 3 for various fibering angles β. In Fig. 3 we observe the following behavior:

- $[\![u_1]\!] = 0$ on Σ and $[\![u_3]\!] < 0$ on Γ_C for all β; $u_1 = u_2 = 0$ for $\beta = 0, \pi/2$; $u_1 < 0$ and $[\![u_2]\!] \geq 0$ on Γ_C for $\beta = \pi/16, \pi/8, \pi/4, 3\pi/8$.
- $\sigma_{21}(u) = 0$ on $\Sigma, \sigma_{23}(u)$ has a r^{-c}-singularity at the crack tip for all β; $\sigma_{22}(u) = 0$ for $\beta = 0, \pi/2$ and otherwise $\sigma_{22}(u) \neq 0$ and it has a r^{-c}-singularity.

On the one hand, this case indicates clearly the appearance of a mixed mode-1 ($[\![u_2]\!] \neq 0$) and mode-3 ($[\![u_3]\!] \neq 0$) crack under pure mode-3 loading. On the other hand, contact between opposite crack surfaces occurs. Both situations are related to the three-dimensional elasticity state showing the advantage of the spatial model with non-penetration conditions, in contrast to plane isotropic ($\beta = 0$) and orthotropic ($\beta = \pi/2$) models. Let us discuss these two effects in more details. First, note that there is no contact between the crack surfaces in the remaining interval $\beta \in (-\pi/2, 0)$. This case was investigated in [24] for the linear problem with the condition $\sigma_{22}(u) = 0$ describing stress-free crack faces $\Gamma_C^{\pm}$. In this reference, for $\beta \neq 0, \pi/2$, the crack also appears in a mixed mode-1 with mode-3 state. Thus, the mode mixing observation is connected inherently with the spatial (coupled) formulation of the composite model which is in contrast to its splitting into independent in-plane and anti-plane states. Secondly, the non-penetration conditions result in a nonlinear model of the composite described by the variational inequality. These conditions need to be considered when contact between opposite crack surfaces occurs within three-dimensional observations.

From the results depicted in Fig. 3, one can see instabilities in $\sigma_{22}(u)$ at the connected part of the interface. This effect shows an oscillatory nature of the constrained components ($[\![u_2]\!]$ and $\sigma_{22}(u)$) of the solution near the crack tip. We emphasize that the exact representation of oscillatory solutions is known analytically for the model of coupled different isotropic materials with interface cracks in the in-plane setting only (see [25]). In the case of the nonlinear model, no such investigations are available in the literature. The oscillations in our case are due to the transmission and non-penetration conditions. A closer investigation of this subject follows in Sect. 3.3.3.

The next section is devoted to a rigorous justification of the numerical technique used. The observations of the nonlinear model continue in Sect. 3.3.

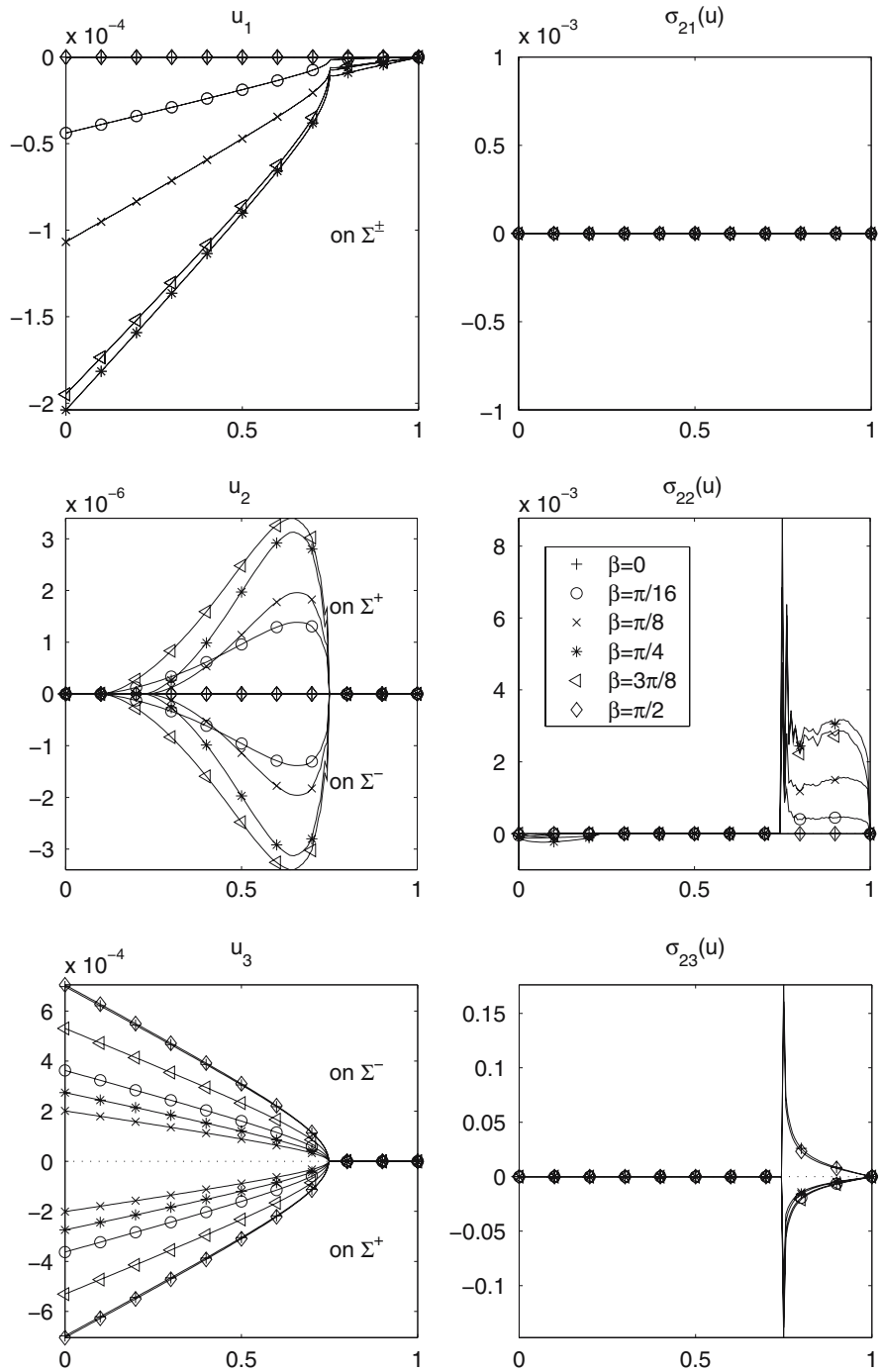

Fig. 3 Displacement and stress at the interface

3 Constrained minimization of the discrete crack problem

The discretization of (2.12) results in an inequality constrained-minimization problem. The first-order optimality conditions are equivalent to a non-differentiable system of equations. Our goal is to use an appropriate extension of Newton's method for the numerical solution. For this purpose, we rely on a

generalization of the classical Frechet-differentiability concept. In fact, we use the following notion introduced in [17]: the operator $F\colon X \to Y$, with X, Y Banach spaces, is called *generalized differentiable* in an open subset $U \subset X$ if there exists mappings $G\colon U \to \mathcal{L}(X, Y)$, referred to as generalized derivatives, such that

$$\lim_{h\to 0} \frac{1}{\|h\|_X} \|F(y+h) - F(y) - G(y+h)h\|_Y = 0 \quad \text{for every } y \in U.$$

Mappings F satisfying this relation are also called *semi-smooth*. In this section, we use the above property in $\mathbb{R}^N$ and construct the resulting semi-smooth Newton algorithm.

3.1 Discretized problem as a linear complementarity system

Discretization of (2.12) results in a quadratic-programming problem of the type

$$\text{minimize } \frac{1}{2}u^\top L u - f^\top u \quad \text{over } u \in \mathbb{R}^N \quad \text{subject to } \Lambda u \geq 0, \tag{3.1}$$

where the symmetric matrix $L \in \mathbb{R}^{N\times N}$ is positive-definite, $f \in \mathbb{R}^N$, and the matrix $\Lambda \in \mathbb{R}^{|B|\times N}$ associated with the non-penetration condition has full column-rank. Here, for the index set $B \subset \{1, \ldots, N\}$, we denote its cardinality by $|B|$. The form of Λ for the specific case of a symmetric partition of the crack surfaces is presented in the numerical examples below.

It is well known that a unique solution $u \in \mathbb{R}^N$ to (3.1) exists and is characterized by the variational inequality (similar to (2.13))

$$\Lambda u \geq 0, \quad (f - Lu)^\top (v - u) \leq 0 \quad \text{for all } v \in \mathbb{R}^N \quad \text{with } \Lambda v \geq 0. \tag{3.2}$$

Introducing a Lagrange multiplier $\lambda \in \mathbb{R}^{|B|}$, we can equivalently express problem (3.1) as: find the pair $(u, \lambda)^\top \in \mathbb{R}^N \times \mathbb{R}^{|B|}$ satisfying the following system of equations (compare with (2.16))

$$Lu - \Lambda^\top \lambda = f, \tag{3.3a}$$

$$\Phi(u, \lambda) := \max(c\lambda - \Lambda u, 0) - c\lambda = 0, \tag{3.3b}$$

where $c > 0$ is an arbitrarily fixed constant. Note that (3.3b) is equivalent to the complementarity system

$$\lambda \geq 0, \quad \Lambda u \geq 0, \quad \lambda^\top (\Lambda u) = 0.$$

Observe also that (3.3) is sufficient for the primal variable u to be the solution of (3.2) and (3.1).

Multiplying (3.3a) first by L^{-1} and then by Λ, we obtain

$$\Lambda u - (\Lambda L^{-1} \Lambda^\top)\lambda - \Lambda L^{-1} f = 0. \tag{3.4}$$

Since the matrix $\Lambda L^{-1} \Lambda^\top$ is positive definite, we can define its inverse which is also a positive definite matrix

$$\hat{L} := (\Lambda L^{-1} \Lambda^\top)^{-1} \in \mathbb{R}^{|B|\times|B|}. \tag{3.5}$$

Setting

$$\hat{u} := \Lambda u \in \mathbb{R}^{|B|}, \quad \hat{f} := \hat{L} \Lambda L^{-1} f \in \mathbb{R}^{|B|}, \tag{3.6}$$

multiplying (3.4) by $\hat{L}$, and taking into account (3.3b), we arrive at the linear complementarity problem for $\hat{u}$ at the subset of indices B only: find $\hat{u} \in \mathbb{R}^{|B|}$ such that

$$\hat{L}\hat{u} - \hat{f} \geq 0, \quad \hat{u} \geq 0, \quad \hat{u}^\top (\hat{L}\hat{u} - \hat{f}) = 0. \tag{3.7}$$

This is the first-order necessary and sufficient optimality condition for the strictly convex quadratic minimization problem

$$\text{minimize } \frac{1}{2}\hat{u}^\top \hat{L}\hat{u} - \hat{f}^\top \hat{u} \quad \text{over } \hat{u} \in \mathbb{R}^{|B|} \quad \text{subject to } \hat{u} \geq 0, \tag{3.8}$$

which admits a unique solution $\hat{u}$. Let $\hat{\lambda}$ denote the multiplier associated with (3.8). Then the pair $(\hat{u}, \hat{\lambda})^\top \in \mathbb{R}^{|B|} \times \mathbb{R}^{|B|}$ satisfies the nonlinear equations analogous to (3.3):

$$\hat{L}\hat{u} - \hat{\lambda} = \hat{f}, \tag{3.9a}$$

$$\hat{\Phi}(\hat{u}, \hat{\lambda}) := \max(c\hat{\lambda} - \hat{u}, 0) - c\hat{\lambda} = 0, \tag{3.9b}$$

with an arbitrarily fixed $c > 0$, where, again, (3.9b) is equivalent to

$$\hat{\lambda} \geq 0, \quad \hat{u} \geq 0, \quad \hat{\lambda}^\top \hat{u} = 0.$$

Lemma 3.1 *Let $(u, \lambda)^\top \in \mathbb{R}^N \times \mathbb{R}^{|B|}$ be the solution of (3.3). Then $\hat{u} = \Lambda u$ and $\hat{\lambda} = \lambda$ solve (3.9). Conversely, let $(\hat{u}, \hat{\lambda})^\top \in \mathbb{R}^{|B|} \times \mathbb{R}^{|B|}$ be the solution to (3.9), then*

$$u = L^{-1}(f + \Lambda^\top \hat{\lambda}) \tag{3.10}$$

and $\lambda = \hat{\lambda}$.

Proof The first assertion of the lemma follows from the discussion of (3.9). To verify the converse assertion, we multiply (3.9a) with $\hat{L}^{-1}$ to obtain

$$\hat{u} - (\Lambda L^{-1} \Lambda^\top)\hat{\lambda} - \Lambda L^{-1} f = 0.$$

From (3.10) and (3.9), we obtain

$$Lu - f - \Lambda^\top \hat{\lambda} = 0, \quad \Lambda u = \hat{u} \geq 0, \quad \hat{\lambda} \geq 0,$$

which (similarly to (3.7)) is the linear complementarity problem associated with (3.3). Now the claim follows from the uniqueness of solution of (3.3). □

The equivalence between (3.3) and (3.9) will be useful for the application of the convergence results of [15,16].

3.2 The primal–dual active-set algorithm as a semi-smooth Newton method

In order to devise a semi-smooth Newton method for solving the constrained minimization problem (3.1), we focus on its primal–dual formulation (3.3). Setting $y := (u, \lambda)^\top \in \mathbb{R}^N \times \mathbb{R}^{|B|}$, we restate the system (3.3) as

$$F(y) := \begin{pmatrix} Lu - \Lambda^\top \lambda - f \\ \Phi(u, \lambda) \end{pmatrix} = 0, \tag{3.11}$$

where the function $F\colon \mathbb{R}^{N+|B|} \to \mathbb{R}^{N+|B|}$ is non-differentiable in the classical sense. However, in the sequel we argue that F is generalized differentiable. For this purpose, we introduce the matrix $\chi_S \in \mathbb{R}^{|B| \times |B|}$ by

$$\chi_S = \operatorname{diag}(s_1, \ldots, s_{|B|}), \quad \text{with } s_i = \begin{cases} 1 & \text{if } i \in S, \\ 0 & \text{if } i \notin S, \end{cases}$$

and define

$$\begin{aligned} A(y) &= \{i \in B : c\lambda_i - (\Lambda u)_i > 0\}, \\ I(y) &= \{i \in B : c\lambda_i - (\Lambda u)_i \leq 0\}. \end{aligned} \tag{3.12}$$

The set $A(y)$ is called the *active* set at y, and $I(y)$ is called the *inactive* set. This terminology is suggested by the fact that $\lambda_i > 0$ and $(\Lambda u)_i = 0$ for all $i \in A(y)$ at the solution y of (3.3). On the other hand, for $i \in I(y)$ we have $\lambda_i = 0$ and $(\Lambda u)_i \geq 0$ at the solution. Definition (3.12) implies that $\chi_{A(y)} + \chi_{I(y)} = 1$. This allows us to rewrite the function Φ in (3.3b) in the form

$$\Phi(u, \lambda) = -\chi_{A(y)} \Lambda u - c\chi_{I(y)} \lambda. \tag{3.13}$$

As a consequence, F in (3.11) admits the representation

$$F(y) = G(y)y - \begin{pmatrix} f \\ 0 \end{pmatrix}, \quad G(y) = \begin{pmatrix} L & -\Lambda^\top \\ -\chi_{A(y)}\Lambda & -c\chi_{I(y)} \end{pmatrix},$$

and satisfies, for small h, the identity

$$F(y+h) - F(y) - G(y+h)h = 0. \tag{3.14}$$

Thus, G in (3.14) serves as a generalized derivative of the non-differentiable mapping F.

Now we can define the semi-smooth Newton method for computing the solution of (3.11): for some initial guess $y^{(0)}$, compute

$$y^{(n+1)} = y^{(n)} - G(y^{(n)})^{-1}F(y^{(n)}), \quad n = 0, 1, \dots . \tag{3.15}$$

As detailed below, each step in (3.15) amounts to solving a well-posed linear system. From [17, Theorem 1.1] the following local convergence result for the process (3.15) can be deduced.

Proposition 3.1 *The semi-smooth Newton iteration* (3.15) *is well defined, and the sequence of iterates* $(y^{(n)})$ *converges superlinearly to a solution* y^* *of* $F(y) = 0$ *provided that* $y^{(0)}$ *is sufficiently close to* y^*.

The numerical implementation of (3.15) is realized as follows:

Algorithm 1

(0) *Choose* $A(y^{(-1)})$ *and* $I(y^{(-1)})$ *such that* $A(y^{(-1)}) \cup I(y^{(-1)}) = B$; *set* $n = -1$.

(1) *Solve for* $y^{(n+1)} = (u^{(n+1)}, \lambda^{(n+1)})^\top \in \mathbb{R}^N \times \mathbb{R}^{|B|}$:

$$Lu^{(n+1)} - \Lambda^\top \lambda^{(n+1)} = f, \tag{3.16a}$$

$$(\Lambda u^{(n+1)})_i = 0 \quad \text{for all } i \in A(y^{(n)}),$$

$$\lambda_i^{(n+1)} = 0 \quad \text{for all } i \in I(y^{(n)}). \tag{3.16b}$$

(2) *Compute the active and inactive sets at* $y^{(n+1)}$:

$$A(y^{(n+1)}) = \{i \in B : \ c\lambda_i^{(n+1)} - (\Lambda u^{(n+1)})_i > 0\}, \tag{3.17a}$$

$$I(y^{(n+1)}) = \{i \in B : \ c\lambda_i^{(n+1)} - (\Lambda u^{(n+1)})_i \le 0\}. \tag{3.17b}$$

(3) *If* $n \ge 0$ *and* $A(y^{(n+1)}) = A(y^{(n)})$ *then STOP*; *else set* $n = n + 1$ *and go to step 1.*

Because Step 2 utilizes both the primal variable u and the dual variable λ, we shall refer to Algorithm 1 as the *primal–dual active set method*. It is equivalent to (3.15): In fact, we start by rewriting (3.15) as

$$L(u^{(n+1)} - u^{(n)}) - \Lambda^\top(\lambda^{(n+1)} - \lambda^{(n)}) = f - Lu^{(n)} + \Lambda^\top\lambda^{(n)}, \tag{3.18a}$$

$$-\chi_{A(y^{(n)})}\Lambda(u^{(n+1)} - u^{(n)}) - c\chi_{I(y^{(n)})}(\lambda^{(n+1)} - \lambda^{(n)}) = c\lambda^{(n)} - \max(c\lambda^{(n)} - \Lambda u^{(n)}, 0). \tag{3.18b}$$

Equation (3.18a) implies (3.16a), and the non-smooth equation (3.18b) is realized by the choices (3.17) and (3.16b).

The stopping rule in Step 3 of Algorithm 1 is motivated by the following considerations. For $i \in A(y^{(n)})$ we have $(\Lambda u^{(n+1)})_i = 0$, and for $i \in I(y^{(n)})$ we obtain $\lambda_i^{(n+1)} = 0$. Hence, if we assume that $A(y^{(n)}) = A(y^{(n+1)})$, then from (3.17a) we infer $\lambda_i^{(n+1)} > 0$ for all $i \in A(y^{(n+1)})$, and $(\Lambda u^{(n+1)})_i \ge 0$ for all $i \in I(y^{(n+1)})$ by (3.17b). This, together with (3.16a), proves that the iterate $y^{(n+1)} = (u^{(n+1)}, \lambda^{(n+1)})^\top$ satisfies $F(y^{(n+1)}) = 0$ if Algorithm 1 terminates in Step 3. This actually occurs in all our numerical examples.

Based on Lemma 3.1, an application of the global convergence results given in [15,16] leads to the following proposition.

Proposition 3.2 *Assume that* $L = M + S$ *with* $M \in \mathbb{R}^{N\times N}$ *a nonsingular* M*-matrix and with* $S \in \mathbb{R}^{N\times N}$ *a perturbation such that* $\|S\|_1$ *is sufficiently small. Then*:

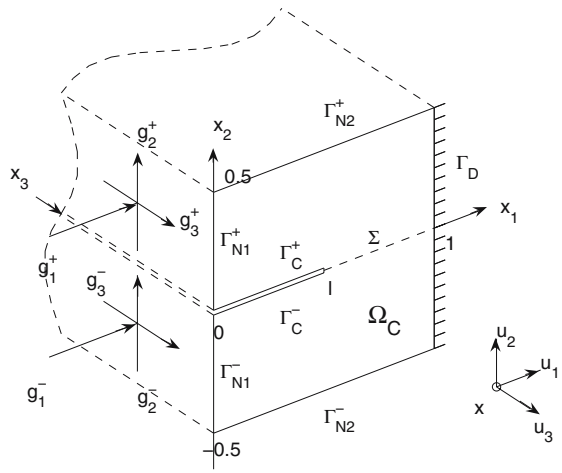

Fig. 4 Geometry of the domain Ω_C

(i) *Regardless of the initial choice, Algorithm 1 is well defined, and the iterates* $(u^{(n)}, \lambda^{(n)})^\top$ *converge to the solution of* (3.3).

(ii) *For the specific initialization of* $\lambda^{(0)} = 0$ *and* $u^{(0)} = L^{-1}f$, *the iterates* $\Lambda u^{(n)}$ *are feasible and they converge monotonically with* $A(y^{(n-1)}) \supset A(y^{(n)})$ *for* $n \geq 1$.

3.3 Observations for a nonlinear model (continued)

Now we give a detailed description of the example presented in Sect. 2.4. The domain Ω is chosen to be a square in $\mathbb{R}^2$ with its boundary decomposed as follows:

$$\Gamma_D = \{x_1 = 1, |x_2| \leq 0.5\}, \quad \Gamma_N = \Gamma_{N1}^+ \cup \Gamma_{N1}^- \cup \Gamma_{N2}^+ \cup \Gamma_{N2}^-,$$
$$\Gamma_{N1}^\pm = \{x_1 = 0, 0 \leq \pm x_2 \leq 0.5\}, \quad \Gamma_{N2}^\pm = \{0 < x_1 < 1, x_2 = \pm 0.5\}.$$

We assume that the crack Γ_C of length $0 < l < L = 1$ is located along a part of the interface, $\Sigma = \{0 < x_1 < 1, x_2 = 0\}$. The corresponding faces in $\Omega^\pm = \Omega \cap \mathbb{R}^2_\pm$ of the crack and the interface are denoted by $\Gamma_C^\pm$ and $\Sigma^\pm$, respectively. The plane domain with crack Ω_C is bounded by Γ_D, Γ_N, and $\Gamma_C^\pm$. The elastic problem (2.8) in Ω_C is considered with the following boundary conditions imposed on Γ_N:

$$\begin{aligned} &\sigma_{12}(u) = \sigma_{22}(u) = \sigma_{23}(u) = 0 \quad \text{on } \Gamma_{N2}^\pm, \\ &-\sigma_{11}(u) = g_1^\pm,\ -\sigma_{12}(u) = g_2^\pm,\ -\sigma_{13}(u) = g_3^\pm \quad \text{on } \Gamma_{N1}^\pm, \end{aligned} \tag{3.19}$$

where we assume anti-symmetric loading corresponding to mode-3:

$$g_3^\pm = \mp g_0, \quad g_1^\pm = g_2^\pm = 0, \quad g_0 = 0.001\mu \approx 3.5376(\text{mPa}), \tag{3.20}$$

as illustrated in Fig. 4.

We utilize the material parameters (2.1) for the specific case (5.3) described in the Appendix with the values from [26]:

$$E_1 = E_2 = E = 10160(\text{mPa}), \quad E_3 = 139400(\text{mPa}),$$
$$G_{31} = G_{32} = G_3 = 4600(\text{mPa}), \quad G_{21} = \frac{E}{2(1+\nu)} \approx 3537.6(\text{mPa}),$$
$$\nu_{21} = \nu = 0.436, \quad \nu_{31} = \nu_{32} = \nu_3 = 0.3.$$

The corresponding minimal eigenvalues $\lambda_{\min}(\beta)$ in (2.15) are found to be positive for $\beta \in [-\pi/2, \pi/2]$. They are approximately constant with value $\lambda_{\min} \approx 3537.6$. In this case (2.14) holds, and the interface crack problem formulated in Sect. 2.3 is well posed.

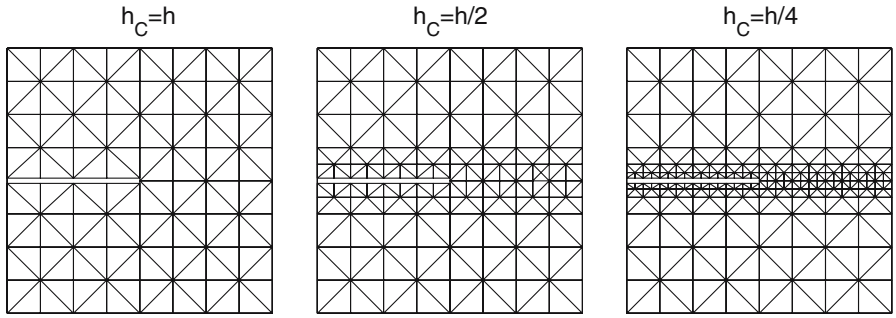

Fig. 5 Meshing in Ω_C for $h = 1/8$

3.3.1 Discretization

We discretize problem (2.8) into finite elements. For the basis functions e^k related to the kth nodal point of the triangulation, we order the displacement vector as

$$\ldots, (u_1)^k, (u_2)^k, (u_3)^k, \ldots, (u_1)^s, (u_2)^s, (u_3)^s, \ldots \ .$$

According to (2.6), the stiffness matrix L in (3.1) involves the following 3×3-cells:

$$\begin{bmatrix} C^\beta_{11} e^k_{,1} e^s_{,1} + C^\beta_{44} e^k_{,2} e^s_{,2} & C^\beta_{12} e^k_{,1} e^s_{,2} + C^\beta_{44} e^k_{,2} e^s_{,1} & C^\beta_{16} e^k_{,1} e^s_{,1} + C^\beta_{45} e^k_{,2} e^s_{,2} \\ C^\beta_{12} e^k_{,1} e^s_{,2} + C^\beta_{44} e^k_{,2} e^s_{,1} & C^\beta_{44} e^k_{,1} e^s_{,1} + C_{22} e^k_{,2} e^s_{,2} & C^\beta_{45} e^k_{,1} e^s_{,2} + C^\beta_{26} e^k_{,2} e^s_{,1} \\ C^\beta_{16} e^k_{,1} e^s_{,1} + C^\beta_{45} e^k_{,2} e^s_{,2} & C^\beta_{45} e^k_{,1} e^s_{,2} + C^\beta_{26} e^k_{,2} e^s_{,1} & C^\beta_{66} e^k_{,1} e^s_{,1} + C^\beta_{55} e^k_{,2} e^s_{,2} \end{bmatrix}$$

Following a common procedure in linear elasticity, we utilize linear finite elements on a triangular mesh constructed in Ω_C. For improved resolution of the singularity (crack tip), which may be located at any point along the interface, we use a local refinement in a neighborhood of Σ. This results in two mesh parameters: h for the uniform mesh in the domain, and h_C for the fine mesh at the interface, as illustrated in Fig. 5 for $h = 1/8$ and $h_C = h, h/2, h/4$. The local refinement is introduced to take into consideration the specific geometry of the coupled domain Ω.

Next, we give the description of the matrix $\Lambda \in \mathbb{R}^{|B| \times N}$ in (3.1) with $B \subset \{1, \ldots, N\}$. First let us define the index set $\mathcal{B} \subset B \times B$. Each pair $(i^+, i^-) \in \mathcal{B}$ corresponds to an index $i \in B$, which belongs to a nodal point at the crack Γ_C, i.e., $i^+ = i^+(i)$ and $i^- = i^-(i)$. Thus, $|\mathcal{B}| = |B|$. This definition allows us to write the discrete non-penetration condition as

$$(u_2)^{i^+} - (u_2)^{i^-} \geq 0 \quad \text{for all } (i^+, i^-) \in \mathcal{B}, \tag{3.21}$$

where $u^{i^\pm} = ((u_1, u_2, u_3)^\top)^{i^\pm}$ are the displacement vectors at the nodal points on Γ_C^+ and Γ_C^-. Secondly, we assume that the vector $u \in \mathbb{R}^N$ is partitioned into $u = (u_D, u_{\tilde{B}})^\top$ with the index set $\tilde{B}$ and the vector $u_{\tilde{B}}$ defined as follows: Let $u_2^{B^+} = ((u_2)^{i^+(1)}, \ldots, (u_2)^{i^+(B)}) \in \mathbb{R}^{|B|}$, and analogously for $u_2^{B^-}$. Then $u_{\tilde{B}} = (u_2^{B^+}, u_2^{B^-})^\top \in \mathbb{R}^{2|B|}$. Thus, we infer that $|\tilde{B}| = 2|B|$. Now, the matrix Λ can be expressed as

$$\Lambda = (\mathbf{0}, \chi_{u_2^{B^+}}, -\chi_{u_2^{B^-}}),$$

where $\mathbf{0}$ is the $|B| \times |D|$-zero matrix with $|D| = N - |\tilde{B}|$. The column-rank of Λ is $|B|$. Therefore, Λ is related to the discretized non-penetration condition (3.21).

3.3.2 Implementation of the primal–dual active-set algorithm

We consider the example of Sect. 2.4. As we shall see the primal–dual active set algorithm possesses the properties stated in Proposition 3.2.

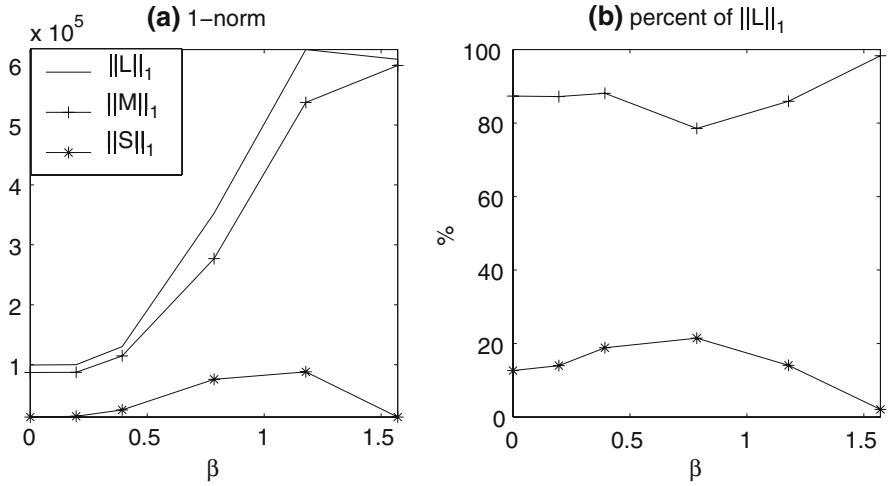

Fig. 6 Decomposition of the stiffness matrix L

Table 1 Number of iterations for fixed grid method

#it/ $h_C =$	1/20	1/40	1/80	1/160	1/320	1/640	1/1280
$h = 1/20$	3	4	5	6	6	–	–
$h = 1/40$	–	4	4	5	7	7	–
$h = 1/80$	–	–	5	5	7	9	9

We decompose the stiffness matrix L as $L = M + S$ with M an M-matrix and S a perturbation. In relation to Proposition 3.2, the 1-norms of L, M, and S are presented in Fig. 6 for a typical value of h and $h/h_C = 4$ for β chosen in $[0, \pi/2]$. These results are independent of h. In the remainder of this section, we fix $\beta = \pi/8$.

In all cases tested, Algorithm 1 terminated after a finite number of iterates by producing the same active/inactive set structure in two consecutive iterations. Thus, it found the exact solution of the discretized problem (3.1). For $l = 0.5$ the number of iterations required for the successful termination of the algorithm is presented in Table 1 for various mesh sizes h and h_C. Table 1 shows that the number of iterations (#it) is rather small and increases moderately when the mesh is refined. We utilized the specific initialization $A(y^{(-1)}) = \emptyset, I(y^{(-1)}) = B$, which corresponds to

$$\lambda^{(0)} = 0, \quad u^{(0)} = L^{-1} f \tag{3.22}$$

in (3.15). We choose c of the order 10^{-8} in the definition of the active and inactive sets in (3.17).

Concerning the monotonicity properties of the Newton iterates, we next present the primal variable $\Lambda u = [\![u_2]\!]$ in (3.21), the dual variable $\lambda = -\sigma_{22}(u)$ according to (2.17), and the characteristic function $\chi_{A(y)}$ of the active set $A(y)$ at the interface Σ, respectively. First let $l = 0.75, h = 1/40$, and $h_C = 1/160$. The iterates $\Lambda u^{(n)}$ and $\lambda^{(n)}$ are depicted in Fig. 7(a) and (b), respectively, for $n = 0, \ldots, 8$. Results are provided only for the interval $x_1 \in [0.22, 0.75]$ near the crack tip where the active/inactive structure is changing. On $x_1 \in [0, 0.22)$ the solution is active for all $n \geq 0$. For convenience, the characteristic function of the active sets $A(y^{(n)})$ for $n = -1, 0, \ldots, 8$ is indicated below the graphs. We observe from Fig. 7 a monotonic behavior of $\Lambda u^{(n)} \geq 0$ and $A(y^{(n-1)})$, but not of $\lambda^{(n)}$. Note further that several grid points are removed from the active set from one iteration to the next.

Results for another set of data with $l = 0.5, h = 1/40$ and $h_C = 1/640$ are presented in Fig. 8 in the interval $[0.42, 0.5]$. The remaining interval $x_1 \in [0, 0.42)$ is split into two subsets: an active and an inactive one near $x_1 = 0$. In Fig. 8 we see also that the active set splits locally near the crack tip into separate intervals. At iteration $n = 6$ the algorithm stops with 2 active and 3 inactive subintervals.

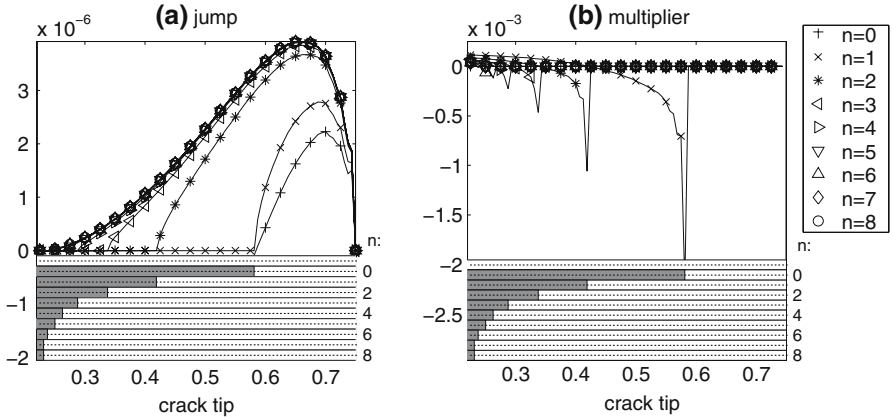

Fig. 7 Iterates $\Lambda u^{(n)}, \lambda^{(n)}$, and $A(y^{(n)})$ for $l = 0.75$

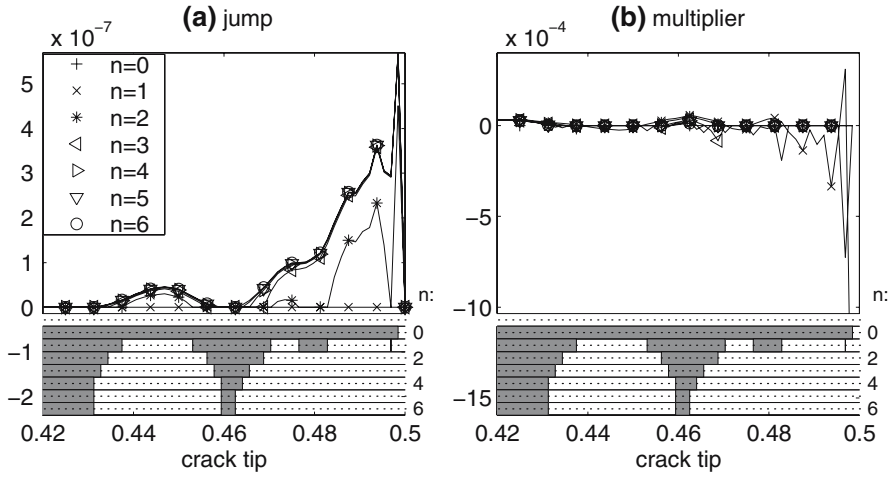

Fig. 8 Iterates $\Lambda u^{(n)}, \lambda^{(n)}$, and $A(y^{(n)})$ for $l = 0.5$

From all examples tested, we can report the following properties of the Newton iterates according to Algorithm 1: the iterates are feasible, i.e., $\Lambda u^{(n)} \geq 0$, and they converge monotonically $\Lambda u^{(n)} \geq \Lambda u^{(n-1)}$ with $A(y^{(n-1)}) \supset A(y^{(n)})$ for $n \geq 1$. This is in accordance with the assertion of Proposition 3.2.

For a reduction of the computational costs, we also used a continuation technique: We solved (3.15) with (3.22) on a coarse grid with $h_C = h$, and subsequently used prolongation of this solution and its corresponding multiplier as initial values on increasingly finer meshes with mesh-size $h_C < h$, respectively. For $l = 0.75$, in Table 2 the first row shows the number of iterations required by Algorithm 1 for a fixed grid. The second row presents the results for the continuation technique. The entry '+2' (or '+1') indicates that only two (or one) iterates are required on the next finer grid for a successful termination with $A(y^{(1)}) = A(y^{(0)})$ (or $A(y^{(0)}) = A(y^{(-1)})$). These results show that the continuation technique is an effective tool for reducing costly fine grid iterations.

3.3.3 Mesh refinement

In this section, we consider the convergence of the results as h and h_C are decreased. For $l = 0.75$ the jump Λu and the corresponding multiplier λ obtained by Algorithm 1 are depicted in Fig. 9(a) and (b). Representative results are shown for $h = 1/40$ with $h_C = 1/40$ and $h_C = 1/640$, and for $h = 1/80$

Table 2 Number of iterations for fixed grid and the continuation method

#it	$h_C =$	1/20	1/40	1/80	1/160	1/320	1/640	1/1280
$h = 1/20$	fixed	5	7	8	9	9	–	–
$h = 1/20$	cont.	5	+2	+2	+2	+2	–	–
$h = 1/40$	fixed	–	7	8	9	10	12	–
$h = 1/40$	cont.	–	7	+2	+2	+2	+2	–
$h = 1/80$	fixed	–	–	8	9	10	11	12
$h = 1/80$	cont.	–	–	8	+2	+1	+2	+2

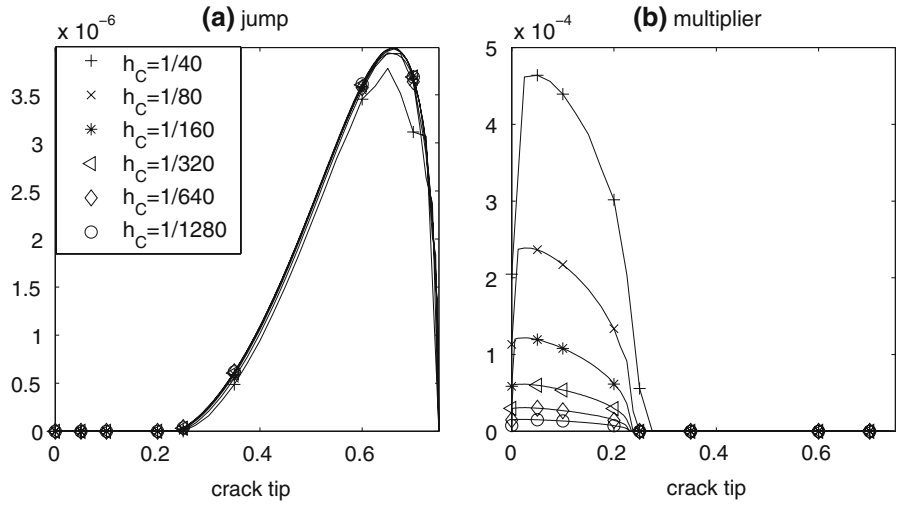

Fig. 9 Solutions Λu and λ for $l = 0.75$

with $h_C = 1/80, 1/160, 1/320, 1/1280$. We see that the solutions Λu are visually almost indistinguishable if $h_C \leq 1/80$, and λ converges monotonically as h_C decreases. The characteristic functions of the corresponding active sets are illustrated in Fig. 10(a). Monotone convergence of $A(y)$ can be observed if both mesh-size parameters decrease.

This is not the case for the crack problem with $l = 0.5$ illustrated in Fig. 10(b). We observe a monotone behavior near the edge $x_1 = 0$, and an oscillation of the active set near the crack tip $x_1 = 0.5$. This behavior persists even when we increase the accuracy `tol` for the iterative solver for the linear system in Step 1 of Algorithm 1. Typically, the outer iteration terminates due to coincidence of two successive iterations. The solutions Λu and λ in the neighborhood of the crack tip at $[0.42, 0.5]$ are depicted in Fig. 11(a) and (b) for $\texttt{tol} \in [10^{-14}, 10^{-8}]$, with the same values for (h_C, h) as stated above. In Fig. 11, again we see an oscillation of the jump $[\![u_2]\!]$ between the corresponding active/inactive intervals. However, we shall see that the solution u itself converges linearly in the energy norm.

To interpret the oscillation effect, let us note that the active set and the crack tip are geometrically separated from each other in the case $l = 0.75$. For $l = 0.5$, however, two geometrical singularities occur simultaneously in a neighborhood of the crack tip: one is connected to the non-penetration conditions resulting in the active set, and the other one is due to the transmission conditions imposed at the joint part of the interface. The phenomenon of oscillation means that in the limit case ($h \to 0$), which corresponds to the continuous problem, it may happen that not only one, but possibly several points (finitely or infinitely many) separate the active/inactive sets which are accumulating in a neighborhood of the crack tip. Alternatively, there may exist a non-zero interval where both the primal and the dual components of the solution are zero, i.e., $[\![u_2]\!] = \sigma_{22}(u) = 0$, (see [25] for an account of oscillations at an interfacial crack).

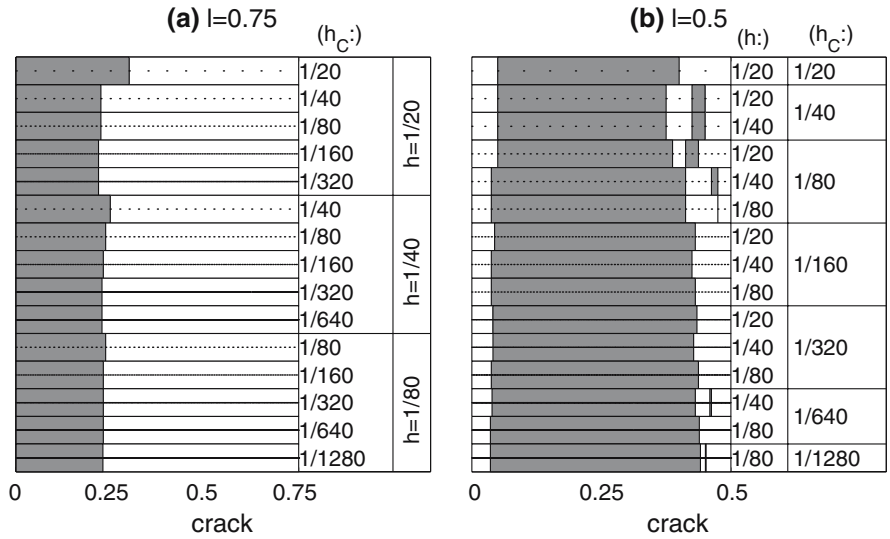

Fig. 10 History of active sets $A(y)$

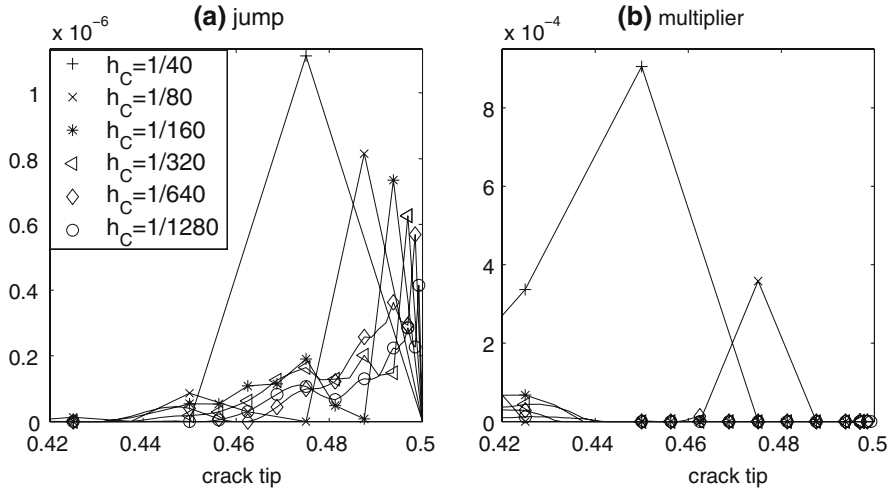

Fig. 11 Solutions Λu and λ for $l = 0.5$

4 Conclusion

In this paper, we have formulated a constrained minimization problem subject to non-penetration conditions to study the nonlinear model of an interface crack in composite materials. In our 2.5-dimensional model, all three components of the displacement vector remain coupled after the assumption of plain deformation. The problem is solved in a two-dimensional cross-section only. This formulation is well suited for the numerical investigations of the three-dimensional phenomenon.

The asymptotic analysis of three-dimensional singularities is not accessible for composite models even in their linearized settings (without the non-penetration conditions). To study the three-dimensional effects we resort to numerical computations based on a primal–dual active set algorithm. The latter numerical technique can be interpreted as a semi-smooth Newton method. It is a reliable and efficient method with fast convergence.

In our numerical experiments, we observe three-dimensional effects of mode mixing, contact of crack surfaces, and its oscillations. All these effects are ruled out for the in-plane and anti-plane isotropic or orthotropic models.

Further, based on our constrained-minimization model, stability properties of the composite with crack can be described, thus predicting the crack growth. This is a highly relevant aspect in fracture mechanics and structure design. By the Griffith fracture hypothesis, the propagation of a crack is determined by the value of energy release rate at the crack tip. It can be argued that the energy release rate is the shape derivative of the potential energy functional with respect to variations of the crack tip. The optimization problem over all admissible crack shapes can be formulated as a minimization of the total potential energy defined as the sum of the potential and the surface energy. Applying the shape optimization approach derived from the Griffith fracture law results in the quasistatic model describing delamination of the composite. The delamination process suggests a predefined path of the crack evolution along the interface. By adopting the primal–dual active-set method, the problem of delamination of composite materials with an interface crack under quasistatic loading is solved numerically in [27].

Acknowledgments This research was supported by the Austrian Science Fund (FWF) in the framework of the research project P18267-N12, the START-program Y305 "Interfaces and Free Boundaries", and the Russian Foundation for Basic Research (project 06-01-00209).

Appendix

The elasticity coefficients in (2.5) have the form (see [23]):

$$
\begin{aligned}
C_{11}^{\beta} &= C'_{33}\sin^4\beta + 2(C'_{13}+2C'_{66})\sin^2\beta\cos^2\beta + C'_{11}\cos^4\beta,\\
C_{66}^{\beta} &= C'_{66} + (C'_{33}+C'_{11}-2C'_{13}-4C'_{66})\sin^2\beta\cos^2\beta,\\
C_{16}^{\beta} &= \left[C'_{11}\cos^2\beta - C'_{33}\sin^2\beta - (C'_{13}+2C'_{66})(\cos^2\beta-\sin^2\beta)\right]\sin\beta\cos\beta,\\
C_{44}^{\beta} &= C'_{44}\cos^2\beta + C'_{55}\sin^2\beta,\\
C_{55}^{\beta} &= C'_{44}\sin^2\beta + C'_{55}\cos^2\beta,\\
C_{45}^{\beta} &= (C'_{44}-C'_{55})\sin\beta\cos\beta,\\
C_{12}^{\beta} &= C'_{23}\sin^2\beta + C'_{12}\cos^2\beta,\\
C_{26}^{\beta} &= (C'_{12}-C'_{23})\sin\beta\cos\beta,\\
C_{22} &= C'_{22}.
\end{aligned}
\tag{5.1}
$$

The primed coefficients referring the rotated coordinate system (x'_1, x'_2, x'_3) connect the material parameters in (2.1) by the relations:

$$
\begin{aligned}
&C'_{11} = \theta\Big(\frac{1}{E_2} - \frac{\nu_{32}^2}{E_3}\Big), \quad C'_{12} = \theta\Big(\frac{\nu_{21}}{E_2} + \frac{\nu_{31}\nu_{32}}{E_3}\Big),\\
&C'_{13} = \theta\Big(\frac{\nu_{31}+\nu_{21}\nu_{32}}{E_2}\Big), \quad C'_{22} = \theta\Big(\frac{1}{E_1} - \frac{\nu_{31}^2}{E_3}\Big),\\
&C'_{23} = \theta\Big(\frac{\nu_{32}}{E_1} + \frac{\nu_{21}\nu_{31}}{E_2}\Big), \quad C'_{33} = \theta\frac{E_3}{E_2}\Big(\frac{1}{E_1} - \frac{\nu_{21}^2}{E_2}\Big),\\
&C'_{44} = G_{21}, \quad C'_{55} = G_{32}, \quad C'_{66} = G_{31},\\
&\frac{1}{\theta} = \Big(\frac{1}{E_2} - \frac{\nu_{32}^2}{E_3}\Big)\Big(\frac{1}{E_1} - \frac{\nu_{31}^2}{E_3}\Big) - \Big(\frac{\nu_{21}}{E_2} + \frac{\nu_{31}\nu_{32}}{E_3}\Big)^2.
\end{aligned}
\tag{5.2}
$$

As specific case, we suppose that the material parameters (2.1) satisfy the identities:

$$E_1 = E_2 = E, \quad \nu_{21} = \nu, \quad G_{21} = \frac{E}{2(1+\nu)},$$
$$\nu_{31} = \nu_{32} = \nu_3, \quad G_{31} = G_{32} = G_3, \tag{5.3}$$

thus reducing the number of independent material parameters to five. These parameters describe a fibering along the x_3'-axis of a material that is isotropic in every plane $x_3' = \text{const}$. With (5.3), we can rewrite (5.2) in the form:

$$C'_{11} = C'_{22} = \kappa \frac{E}{1+\nu}\Big(\frac{1}{E} - \frac{\nu_3^2}{E_3}\Big), \quad C'_{12} = \kappa \frac{E}{1+\nu}\Big(\frac{\nu}{E} + \frac{\nu_3^2}{E_3}\Big),$$
$$C'_{13} = C'_{23} = \kappa\nu_3, \quad C'_{33} = \kappa \frac{E_3}{E}(1-\nu),$$
$$C'_{44} = \frac{E}{2(1+\nu)}, \quad C'_{55} = C'_{66} = G_3, \tag{5.4}$$
$$\frac{1}{\kappa} = \frac{1-\nu}{E} - \frac{2\nu_3^2}{E_3} = \Big(\frac{1}{E} - \frac{\nu_3^2}{E_3}\Big) - \Big(\frac{\nu}{E} + \frac{\nu_3^2}{E_3}\Big).$$

Note that the coefficients in (5.4) fulfill the relations:

$$C'_{12} + 2C'_{44} = C'_{11} = C'_{22}, \quad C'_{12} + C'_{44} = 0.5\kappa. \tag{5.5}$$

In what follows, we consider the two limit cases $\beta = 0$ and $\beta = \pm\pi/2$. For $\beta = 0$ we introduce the Lamé parameters:

$$\mu = \frac{E}{2(1+\nu)}, \quad \lambda = \kappa \frac{E}{1+\nu}\Big(\frac{\nu}{E} + \frac{\nu_3^2}{E_3}\Big). \tag{5.6}$$

In this case, from (5.5) and (5.6) we obtain $\kappa = 2(\lambda+\mu)$, and the coefficients in (5.1) are given by

$$C^0_{11} = C_{22} = \lambda + 2\mu, \quad C^0_{12} = \lambda, \quad C^0_{44} = \mu,$$
$$C^0_{55} = C^0_{66} = G_3, \quad C^0_{16} = C^0_{26} = C^0_{45} = 0. \tag{5.7}$$

Using (5.7), the stress in (2.6) is split into the components for $(u_1, u_2)^\top$:

$$\sigma^0_{11}(u) = C^0_{11}u_{1,1} + C^0_{12}u_{2,2},$$
$$\sigma^0_{22}(u) = C^0_{12}u_{1,1} + C_{22}u_{2,2}, \tag{5.8}$$
$$\sigma^0_{12}(u) = C^0_{44}(u_{1,2} + u_{2,1}),$$

and independent components for u_3:

$$\sigma^0_{23}(u) = C^0_{55}u_{3,2}, \quad \sigma^0_{13}(u) = C^0_{66}u_{3,1}. \tag{5.9}$$

Hence, from (5.8) and (5.9) we arrive at a two-dimensional Lamé/Laplace operator in (2.9) for the in-plane/anti-plane isotropic problem:

$$\sigma^0_{1\alpha,\alpha}(u) = \mu\Delta u_1 + (\lambda+\mu)(\operatorname{div} u)_{,1},$$
$$\sigma^0_{2\alpha,\alpha}(u) = \mu\Delta u_2 + (\lambda+\mu)(\operatorname{div} u)_{,2},$$
$$\sigma^0_{3\alpha,\alpha}(u) = G_3\Delta u_3,$$

where $\operatorname{div} u = u_{1,1} + u_{2,2}$ and $\Delta u_i = u_{i,11} + u_{i,22}, i = 1,2,3$.

Next, consider the case $\beta = \pm\pi/2$. From (5.1) and (5.3), we derive

$$
\begin{aligned}
&C_{11}^{\pm\pi/2} = \kappa\frac{E_3}{E}(1-\nu), \quad C_{22} = \kappa\frac{E}{1+\nu}\Big(\frac{1}{E} - \frac{\nu_3^2}{E_3}\Big),\\
&C_{12}^{\pm\pi/2} = \kappa\nu_3, \quad C_{55}^{\pm\pi/2} = \frac{E}{2(1+\nu)}, \quad C_{44}^{\pm\pi/2} = C_{66}^{\pm\pi/2} = G_3,\\
&C_{16}^{\pm\pi/2} = C_{26}^{\pm\pi/2} = C_{45}^{\pm\pi/2} = 0.
\end{aligned}
\tag{5.10}
$$

According to (5.10), the stress tensor (2.6) is split as in (5.8) and (5.9). As a result, we arrive at the following operator in (2.9) for the in-plane/anti-plane orthotropic problem:

$$
\begin{aligned}
\sigma_{1\alpha,\alpha}^{\pm\pi/2}(u) &= \kappa\frac{E_3}{E}(1-\nu)u_{1,11} + G_3u_{1,22} + (\kappa\nu_3 + G_3)u_{2,12},\\
\sigma_{2\alpha,\alpha}^{\pm\pi/2}(u) &= (\kappa\nu_3 + G_3)u_{1,12} + G_3u_{2,11} + (2\mu+\lambda)u_{2,22},\\
\sigma_{3\alpha,\alpha}^{\pm\pi/2}(u) &= G_3u_{3,11} + \mu u_{3,22}.
\end{aligned}
$$

We conclude that the spatial model under consideration is intermediate between the plane isotropic model for $\beta = 0$ and the plane orthotropic model for $\beta = \pm\pi/2$.

References

1. Lur'e AI (1964) Three-dimensional problems in the theory of elasticity. Interscience, New York
2. Cherepanov GP (1979) Mechanics of brittle fracture. McGraw-Hill, New York
3. Morozov NF (1984) Mathematical foundation of the crack theory. Nauka, Moscow (in Russian)
4. Davidson BD, Krüger R, König M (1995) Three-dimensional analysis of center-delaminated unidirectional and multidirectional single-leg bending specimens. Comp Sci Technol 54:385–394
5. Byron Pipes R, Pagano NJ (1970) Interlaminar stresses in composite laminates under uniform axial extension. J Comp Mater 4:538–548
6. Khludnev AM, Kovtunenko VA (2000) Analysis of cracks in solids. WIT-Press, Southampton Boston
7. Khludnev AM, Sokolowski J (1999) The Griffith formula and the Cherepanov-Rice integral for crack problems with unilateral conditions in nonsmooth domains. Eur J Appl Math 10:379–394
8. Ting TCT (1986) Explicit solution and invariance of the singularities at an interface crack in anisotropic composites. Int J Solids Struct 22:965–983
9. Nazarov SA (1998) The interface crack in anisotropic bodies: stress singularities and invariant integrals. J Appl Maths Mech 62:453–464
10. Mifflin R (1977) Semismooth and semiconvex functions in constrained optimization. SIAM J Control Optim 15:959–972
11. Klatte D, Kummer B (2002) Nonsmooth equations in optimization. Kluwer Publishers, Dordrecht
12. Ulbrich M (2003) Semismooth Newton methods for operator equations in function spaces. SIAM J Optim 13:805–842
13. Cottle RW, Pang J-S, Stone RE (1992) The linear complementarity problem. Academic Press, Boston
14. Hintermüller M, Kovtunenko VA, Kunisch K (2004) The primal–dual active set method for a crack problem with non-penetration. IMA J Appl Math 69:1–26
15. Hintermüller M, Kovtunenko VA, Kunisch K (2004) Semismooth Newton methods for a class of unilaterally constrained variational problems. Adv Math Sci Appl 14:513–535
16. Hintermüller M, Kovtunenko VA, Kunisch K (2005) Generalized Newton methods for crack problems with non-penetration condition. Numer Methods Partial Differential Equations 21:586–610
17. Hintermüller M, Ito K, Kunisch K (2003) The primal–dual active set strategy as a semismooth Newton method. SIAM J Optim 13:865–888
18. Ito K, Kunisch K (2003) Semi-smooth Newton methods for the variational inequalities of the first kind. ESAIM, Math Model Numer Anal 37:41–62
19. Leontiev A, Herskovits J, Eboli C (1998) Optimization theory application to splitted plane bending problems. Int J Solids Struct 35:2679–2694
20. Belhachmi Z, Sac-Epée JM, Sokolowski J (2005) Mixed finite elements methods for smooth domain formulation of crack problems. SIAM J Numer Anal 43:1295–1320
21. Moës N, Dolbow J, Belytschko T (1999) A finite element method for crack growth without remeshing. Int J Numer Math Engng 46:131–150
22. Sukumar N, Moës N, Moran B, Belytschko T (2000) Extended finite element method for three-dimensional crack modelling. Int J Numer Math Engng 48:1549–1570

23. Lekhnitskii SG (1963) Theory of elasticity of an anisotropic body. Holden-Day, San Francisco
24. Kovtunenko VA (2006) Interface cracks in composite orthotropic materials and their delamination via global shape optimization. Optim Eng 7:173–199
25. Rice JR (1988) Elastic fracture mechanics concepts for interfacial cracks. Trans ASME Ser E J Appl Mech 55:98–103
26. König M, Krüger R, Kussmaul K, von Alberti M, Gädke M (1997) Characterizing static and fatigue interlaminar fracture behavior of a first generation graphite/epoxy composite. In: Hooper JS (ed) 13th Composite materials: testing and design 13, ASTM STP 1242, ASTM, 60–81
27. Hintermüller M, Kovtunenko VA, Kunisch K (2006) An optimization approach for the delamination of a composite material with non-penetration. In: Glowinski R, Zolesio J-P (eds) Free and moving boundaries: analysis, simulation and control, Lecture Notes in Pure and Applied Mathematics 252. Chapman & Hall/CRC (to appear)